

Supplementary Information for
**Epitope Fluctuations in the Human Papillomavirus Are Under Allosteric Control – A
Computational Evaluation of a New Vaccine Design Strategy**

Abhishek Singharoy[†], Abhigna Polavarapu[†], Harshad Joshi[†], Mu-Hyun Baik^{†,‡,} and Peter Ortoleva^{†,*}*

[†]Department of Chemistry, Indiana University, 800 E. Kirkwood Avenue, Bloomington, IN 47405, USA,
and

[‡]Department of Materials Chemistry, Korea University, Jochiwon-eup, Sejong-si, 339-700,
South Korea.

E-mail: mbaik@indiana.edu; ortoleva@indiana.edu

Table of Contents

I. Force Field Development	2
II. Molecular Dynamics Simulation Details.....	2
III. Hybrid Design Principles.....	3
IV. Thermodynamic Nature of Allosteric Signal Transduction	4
V. Curved versus Flat Silica Surface.....	5
VI. Figures and Tables	6

I. Force Field Development

A systematic procedure as demonstrated in MacKerell's paper¹ was followed to develop force fields for the organic tether attached to silica surface. For simulating the silica surface, force fields parameters developed by MacKerell's group were used. The parameters of the silicon atom attached to the tether have been modified during the optimization of tether parameters. A small model of the tether attached to silica, represented in Figure S1a was used to parameterize the force fields. Initially the structure of the tether is optimized using density functional calculations² at the B3LYP^{3,4} level. Optimized structure of the tether is then used for force field parameterization with CHARMM27⁵ force fields. Available CHARMM27 parameters^{6,7} for similar organic compounds and silica were introduced as the guess parameters for the first optimization step. The structure was then calculated with the new MM force fields for validating the guess parameters. Charges on the atoms were derived from Merz-Kollman ESP charges⁸ obtained from QM calculations with Gaussian 03⁹ package. After several cycles of optimizing the parameters, reproducibility of target QM bond lengths, bond angles and vibrational spectra have been tested. Figure S1b shows the comparison of structures obtained from QM and MM calculations, and Figure S2 shows the correlation between normal modes for simulations with QM and MM methods. In Table S1 bond lengths and angles are compared between the QM and MM methods. The new force field parameters are tabulated in Table S2.

II. Molecular Dynamics Simulation Details

All simulations were performed with the MD software NAMD 2.7¹⁰ using the CHARMM force field¹¹ for proteins and silica along with the ones developed above for the tether. The TIP3P¹² model is used to simulate water. The constructs were solvated in a cubic box with 20Å thick layers of water along the three Cartesian directions. Consequently the simulated system size varied from $\sim 10^5$ to $\sim 10^6$ atoms. The systems were kept at constant temperature using Langevin dynamics for all non-hydrogen atoms with a Langevin damping coefficient of 5ps^{-1} . A constant pressure of 1atm was maintained using the Nose-Hoover Langevin piston¹³ with a period of 100fs and damping timescale of 50fs. As is done in other studies¹⁴, for all the simulations, only surface layer silica dynamics is considered; all subsequent layers are held fixed.

Simulations were performed with an integration time step of 1fs where bonded interactions were computed every time step, short-range non-bonded interactions every two time steps, and long range electrostatic interactions every four time steps. A cutoff of 12Å was used for van der Waals and short-range electrostatic interactions: a switching function was started at 10 Å for van der Waals interactions to ensure a smooth cutoff. The simulations were performed under

periodic boundary conditions, with full-system, long-range electrostatics calculated by using the PME method with a grid point density of $1/\text{\AA}$. The unit cell was large enough so that adjacent copies of the system did not interact via short-range interactions. Prior to simulation, each system was subjected to 1000 steps of conjugate gradient energy minimization, followed by 100ps of equilibration. We then performed 10ns of MD on each of the systems described above at 300K.

To confirm allosteric interactions between the h4 helix and the epitopes, the isolated L1 protein is simulated by artificially removing or constraining the h4 helix comprising residue 414 to 434. The simulation is performed on NAMD using parameters as described above. NAMD actually calculates the constraints potential with $U = k(x-x_0)^d$. Exponent for harmonic constraint energy function is chosen to be the default 2, and k is chosen to be 5; higher values of k are avoided as they lead to numerical instability in NAMD. With these settings, the atoms of the helix residues are effectively subjected to a constraining potential of $10 \text{ kcal mol}^{-1}\text{\AA}^{-2}$. At 300K, such constraints imply a mean displacement of 0.1-0.3 \AA per atom. Such motions are much lesser than the positional variance of the h4 helix as shown in Figure S5b. Consequently, motion of the h4 helix is ceased yet overall L1 protein movement in the aqueous solution is not disturbed. Subsequent effect on epitope behavior is studied as presented in the Results and Discussion of the article.

III. Hybrid Design Principles

The proposed hybrid designs involve L1 protein or pentamers attached to a silica surface using covalent $-(\text{CH}_2)_3\text{-NH}_2-$ tethers. Using silica in the hybrid design has the following advantages. First, surface properties are sufficiently adjustable to hold small molecules or larger nanostructures.¹⁵ Consequently, silica-based nanoparticles/nanobeads are very useful in bioanalysis once conjugated with biological entities for analyte recognition and/or signal generation. Second, silica nanomaterials are effectively “transparent”. They are unlikely to absorb light in the near-infrared, visible and ultraviolet regions or to interfere with magnetic fields, which allows the functional groups inside silica matrix to keep their original optical and magnetic properties; this facilitates use of lighter magnetic fields during medical procedures.¹⁶⁻¹⁸ Third, silica matrices are highly nontoxic and biocompatible. Furthermore, well-established silica surface-chemistry facilitates the modification of silica-based nanohybrids.¹⁹ Finally, to enable computer-aided design, dependable all-atom force fields are available for silica- water, ion and biomolecule simulations.^{1,20} Also, silica surface has negative potential due to the presence of hydroxyl groups, and therefore electrostatically binds to the inner surface of an L1 protein or pentamer. In a virus, the protein capsid encloses negatively charged DNA or RNA. The latter electrostatically stabilize the assembly through interactions with the inner capsid surface. As used in applications such as

nanotemplating^{15,21} and in delivery agents,²² within hybrid material design, the negatively surface charged silica plays the stabilizing role of the viral genome. However, like most other nanomaterials, including gold or magnetic nanoparticles, and quantum dots, silica particles are difficult to directly and uniformly suspend in aqueous solutions of different salinity. One option to overcome these limitations is to coat these materials with a more stable and physically adaptive material.^{19,21} This way, stoichiometrically defined nanoparticles with correctly oriented immobilized biological elements are obtained.¹⁵ For the present simulation, the silica surface is functionalized with aliphatic-amino tethers.

IV. Thermodynamic Nature of Allosteric Signal Transduction

The allosteric signals are commonly known to follow enthalpic, entropic, or combined pathways.²³ The enthalpic changes involve large scale domain motions in the active site (epitopes here) and associated change in backbone dihedrals. In the present case, the epitope region of free L1 protein undergoes a close-to-open transition as it is removed from its confined state within the T=1 VLP. However, this transition is independent of the helix-epitope allostery as it exists even in the helix frozen or truncated free L1 protein (Figure S4). The average conformation of the epitopes shows strong overlap between the immune responsive (T=1 VLP) and irresponsive (free and pentamer) states of the L1 protein (Figure S3a and c). This overlap is more pronounced between the pentamer and the VLP. Similarly, the epitope energy distribution encompasses a comparable range of values for the monomer, pentamer and VLP. However, the distribution narrows as L1 assembly size increases, implying their repressed fluctuation, yet comparable average epitope structure (Figure S5a). This suggests the present h4 mediated allostery does not control strong changes in structure of the epitope; rather it involves changes in epitope activity as manifested by fluctuations (Figures 4 and 6). Thus, the observed allosteric pathway is possibly entropy-driven. Rather than shifting the free energy minimum in the phase space, which manifests in large scale geometric changes, the allosteric signal induces a change in the depth of the corresponding free energy well mediated exclusively by changes in high frequency protein motion. (i.e., the increased role of entropy implies a flattening of the free energy landscape and thereby the well depth).²³ Generally, such entropy mediated signal transduction is found between physically close sites.²⁴ However, information transfer over long distances is achieved through channels created by helical coils.²⁵ Such entropy transfer is enabled by the increased stiffness of these coils. In the present case, the beta sheets connect h4 helices with the epitopes. In analogy to ref. 25, their stiffness increases and correlation with h4 decreases as the L1 proteins are packed in an assembly (Figure S5b). This additional stiffness of the beta sheets can facilitate entropy transfer between the allosteric and active sites. Conversely, correlations between the h4 helix, beta sheet and epitopes, and associated motions increase in an isolated L1 protein. With this, a part of the helix energy can be dissipated through the beta sheet as information is transferred

from the helix to the epitopes. Consequently, epitopes of an isolated L1 monomer are marginally higher in energy than those of larger L1 assemblies (Figure S5a) as observed in associated power spectrum (Figure S3).

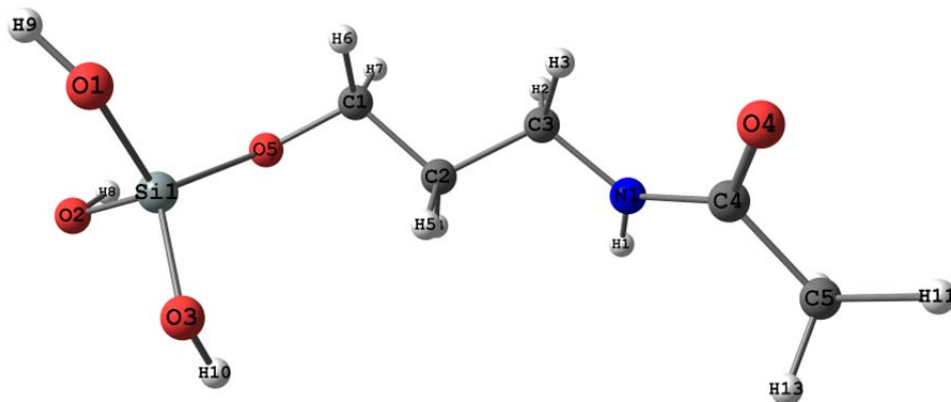
V. Curved versus Flat Silica Surface

The L1 pentamer with positive potential surface was attached to the silica surface possessing negative electrostatic surface potential (Figure S8). The epitope fluctuation characteristics of this design are very close to those from the full VLP (Figure 6) and similarly for helix-epitope correlations. However, a closer look into epitope properties reveals that they are different from those of the VLP. For example, the number of inter-epitope contacts and hydrogen bonds is lower than those in the T=1 VLP (Figure S8). As the pentamer is computationally extracted from a VLP it expands to a new equilibrium structure. When the expanded pentamer is attached to a flat silica surface, its inherent curvature and associated inter-L1 contact (which mediate epitope properties) is lost. In particular, a large fraction of the inter-epitope hydrogen bonds connecting the FG and HI loops is lost. Thus, the fluctuations are also marginally higher in specific regions of the epitope. For example, THR residue 266 in the FG loops consistently loses hydrogen bonding interactions with the ASN residue 357 of the HI loop from its clockwise neighbor, thereby fluctuating more than in a complete VLP (Figures 6). Implications of residue-level conformations, such as those of THR 266, on the immunogenicity of associated constructs are discussed in the main text in the light of experimental findings. In conclusion, properties of the pentamer-flat silica design indicate that, in addition to confinement, inter-L1 interactions and helix-epitope allostery, one must consider surface curvature of the silica nanoparticle, as it plays a crucial role in determining epitope dynamics.

To quantify this finding, the effect of silica surface curvature is investigated. Silica surface curvature chosen to be that of the T=1 VLP so that the bound pentamer maintains its inherent curvature. This design reproduces all epitope properties of the VLP, as is reflected in the positional variance (Figure 6), dihedral distribution, correlation plot, number of hydrogen bonds, contact analysis and epitope energetics (Figures S8, S9 and S10).

VI. Figures and Tables

(a)



(b)

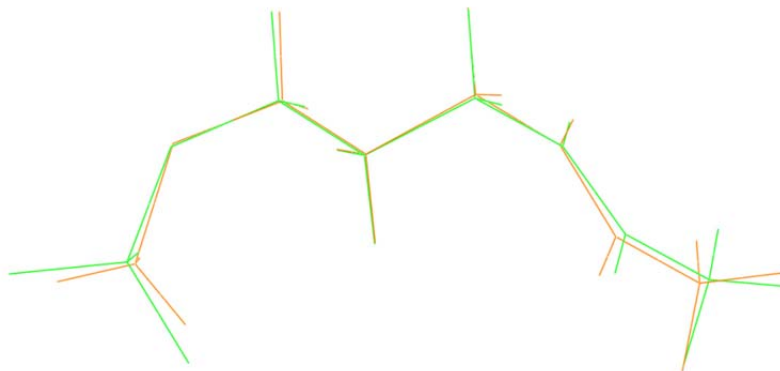


Figure S1. (a) QM Model of the tether bound to silica. (b) Comparison of QM structure (Red) of tether to that of MM optimized structure (Green) with the new force fields.

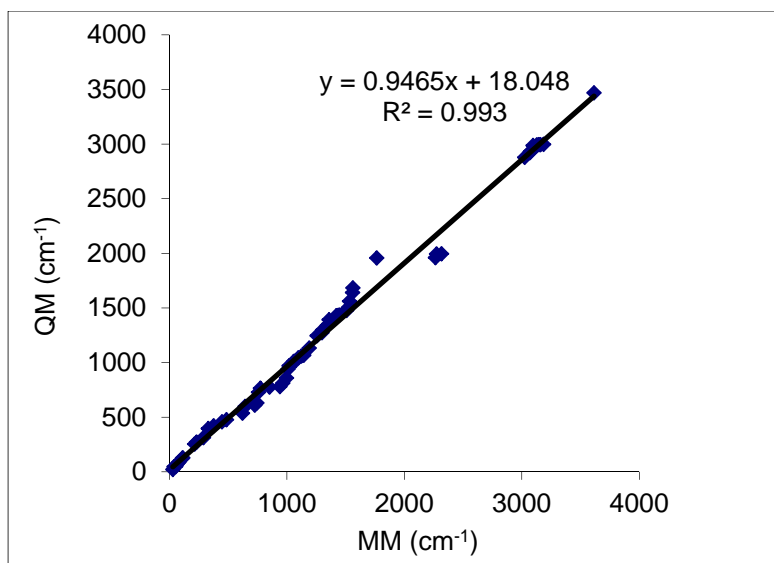


Figure S2. Correlation of vibrational frequencies obtained from QM and MM normal mode calculations.

Table S1. Comparison of bond lengths (Å) and bond angles (°) of QM and MM optimized structure using the newly developed MM force fields.

Bond Length	MM	QM
Si1-O2	1.67	1.67
O2-C1	1.43	1.43
C1-C2	1.51	1.52
C2-C3	1.51	1.53
C3-N1	1.44	1.45
N1-C4	1.37	1.37
C4-C5	1.50	1.51
Bond Angle	MM	QM
Si1-O2-C1	119.4	121.7
O2-C1-C2	111.0	111.8
C1-C2-C3	108.7	111.8
C2-C3-N1	111.3	112.8
C3-N1-C4	119.9	120.4
N1-C4-C5	114.5	115.5

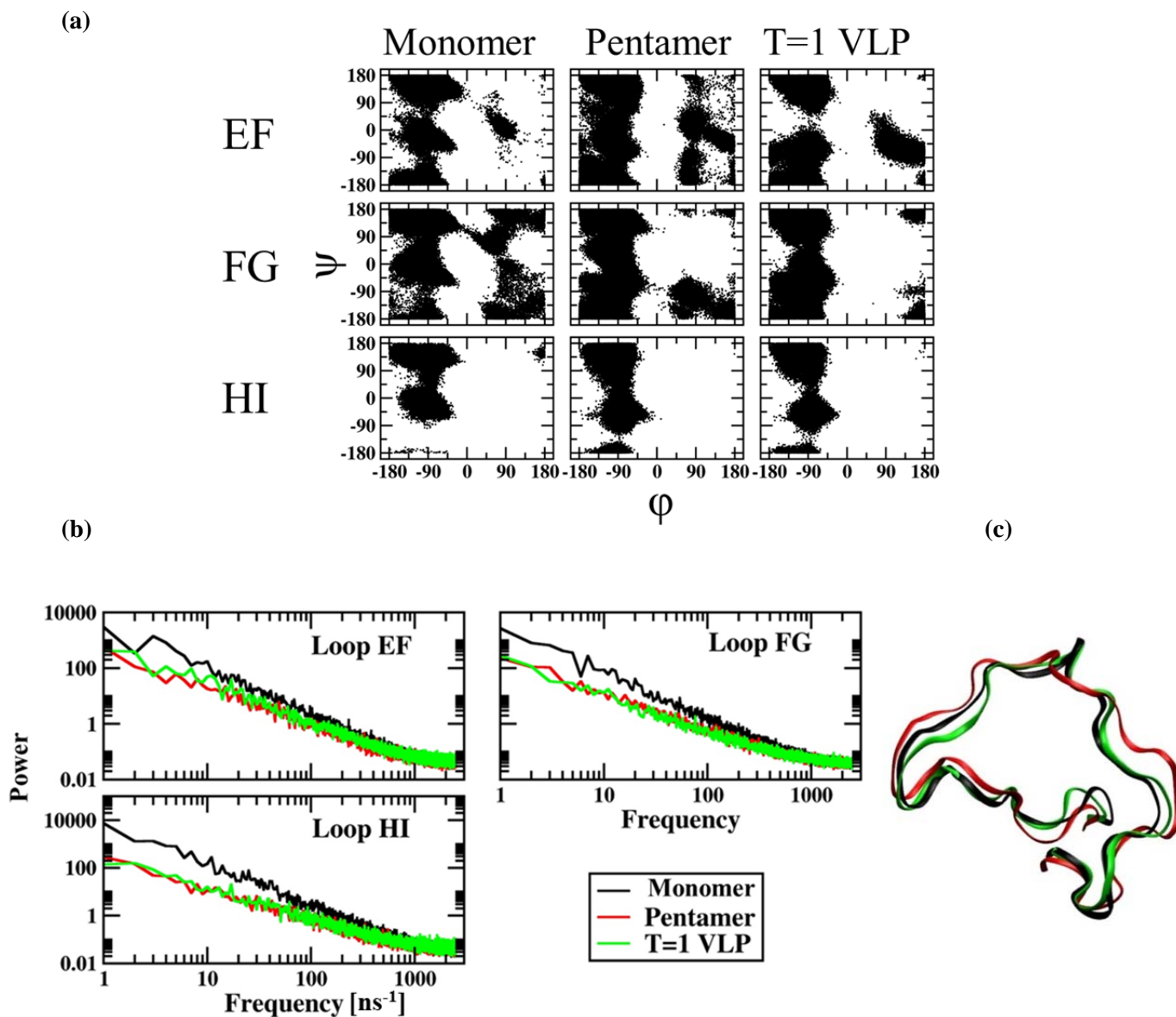


Figure S3. (a) Loop dihedral distribution for monomer (left), pentamer (middle) and the T = 1 VLP (right). Distributions are shown for EF (first row), FG (second row), and HI (third row). For each loop the x -axis (ϕ angle) and corresponding y -axis (ψ angle) specifies positions in the dihedral space. In general, the spread of the distributions decrease as the assembly size increases. (b) Power spectrum for fluctuations in three loops: EF, FG, and HI. Frequency of the loop conformational fluctuations is indicated on x -axis while their averaged square magnitude is indicated on y -axis. Spectra for L1 monomer, pentamer and T = 1 VLP are indicated in black, red and green, respectively. (c) Mean orientation of the epitopes suggesting they change minimally between the monomer (blue), pentamer (red) and VLP (green).

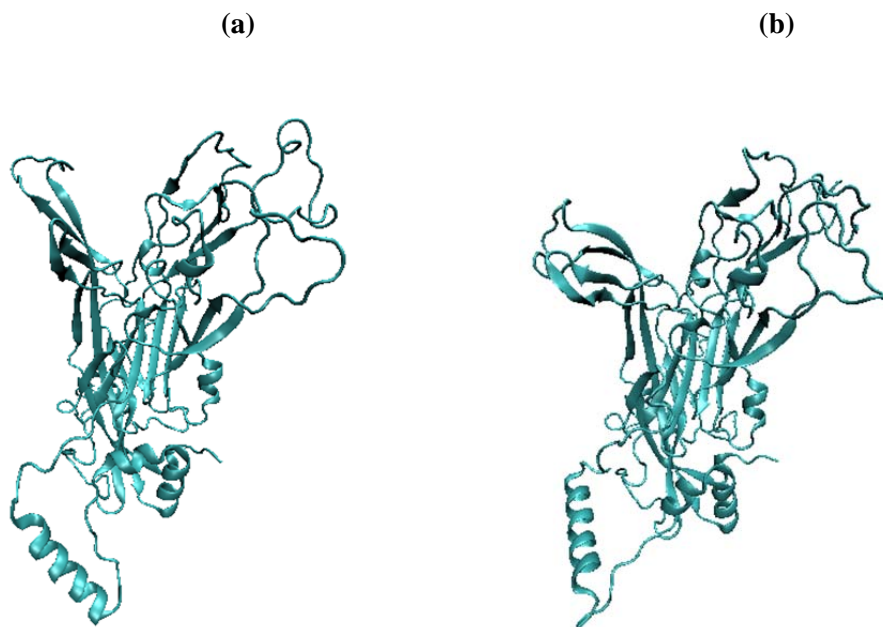


Figure S4. Close (a) to open (b) transition in epitope region of the free L1 protein after it is removed from its confined state within the T=1 VLP.

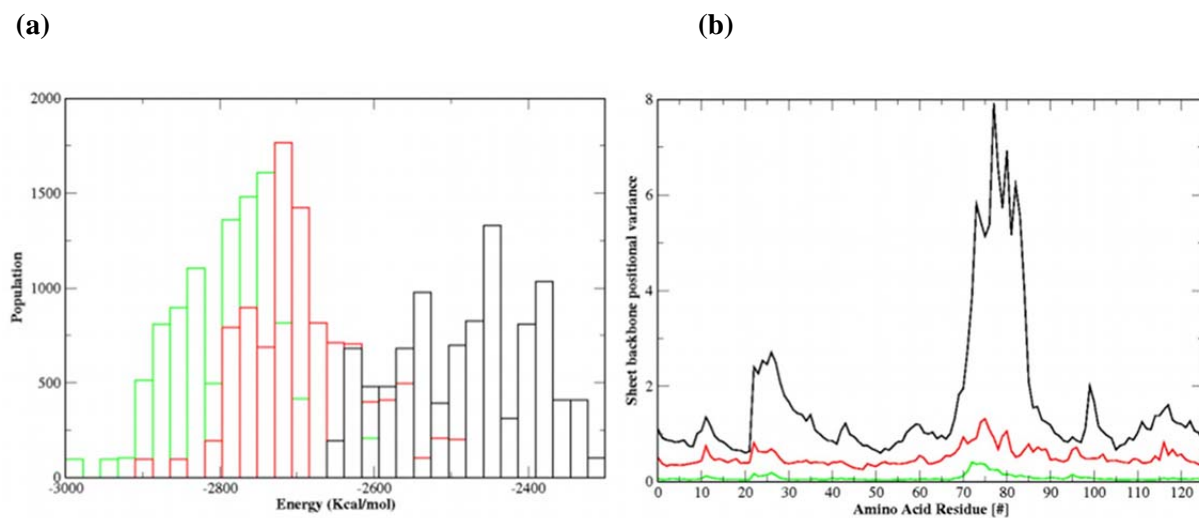


Figure S5. (a) Energy distribution of the epitopes showing they sample similar range of energy values, however, the peak shifts gradually to lower values and is more distinct for those on the T=1 VLP as compared to the pentamer and protein (color code is same as in Figure 3); histograms include 10^4 data points saved every ps from the 10ns trajectories. (b) Positional variance of the sheets that join epitopes to

the h4 helices decreases with increase in confinement and assembly size. These results suggest a primarily entropic pathway for the observed helix-loop allostery in the L1 pentamer and VLP. Marginally higher epitope energies in free L1 protein suggest associated allosteric interactions express significant enthalpic contribution.

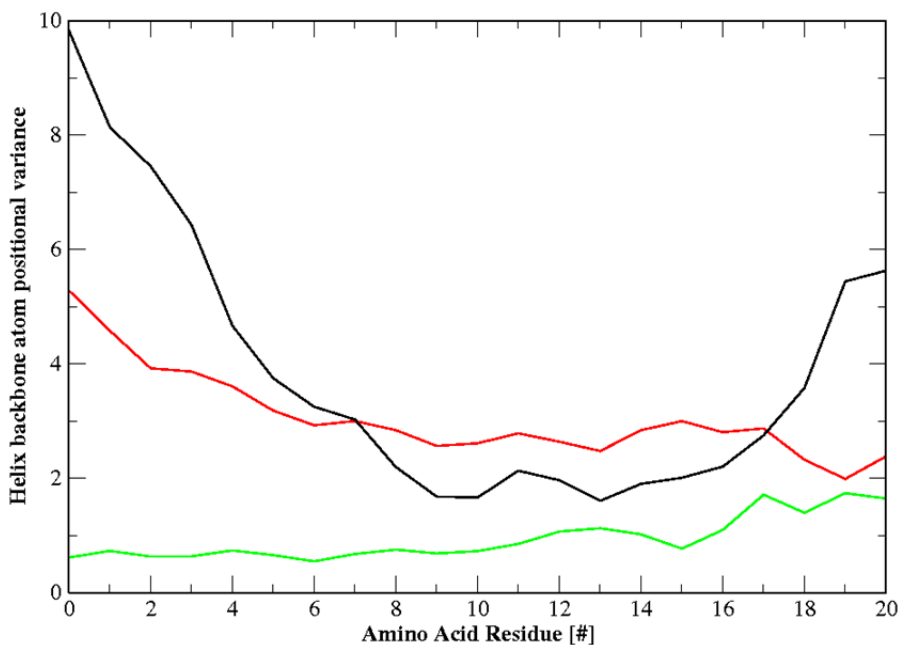


Figure S6. Decrease in helix backbone fluctuation from L1 to pentamer to VLP showing fluctuation-immunogenicity hypothesis still holds if h4 is considered an epitope. Consequently h4 serves as an indispensable part of an HPV vaccine, and therefore has been considered in our silica-based designs.

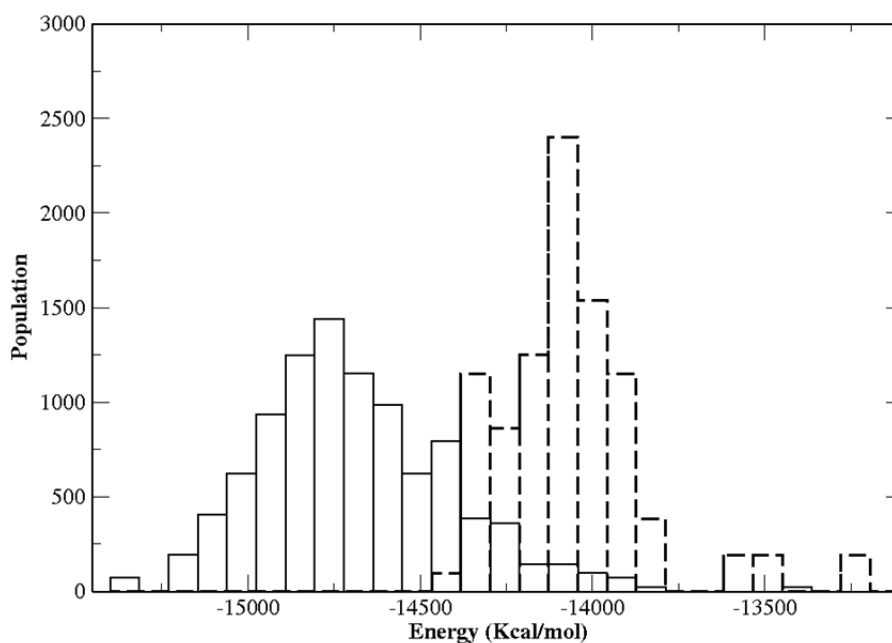


Figure S7. The h4 helix is more stabilized in the horizontal (solid, Figure 5b) versus vertical (dashed, Figure 5a) configuration on the hydrophilic 100 silica surface. Consequently, design E is more probable than D.

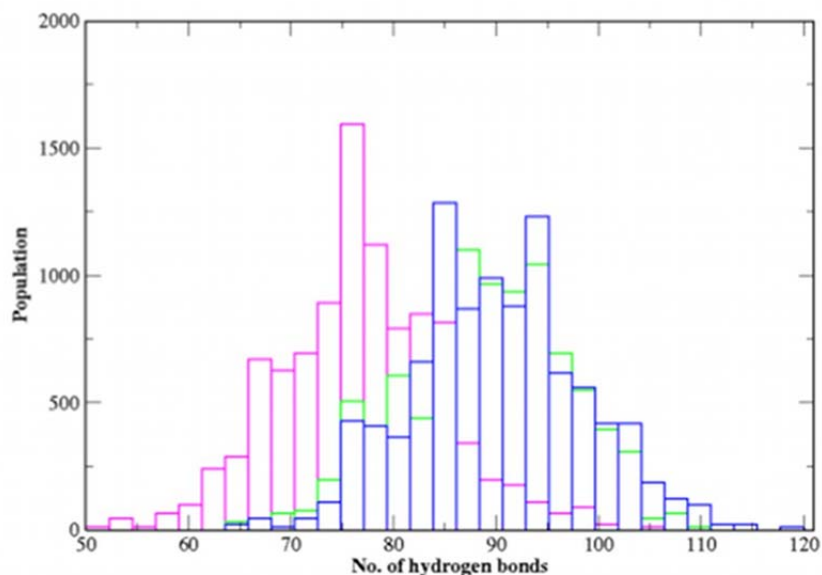


Figure S8. Epitope, FG, hydrogen bond distributions showing pentamer on a flat silica surface (magenta) has lesser number of hydrogen bonds than on a curved one (blue); hydrogen bond distribution of FG from the pentamer-curved silica construct is comparable to that from the T=1 HPV VLP. This loss of hydrogen bonds is attributed to alternations in inter L1 contact as curvature of the pentamer changes (Figure S10).

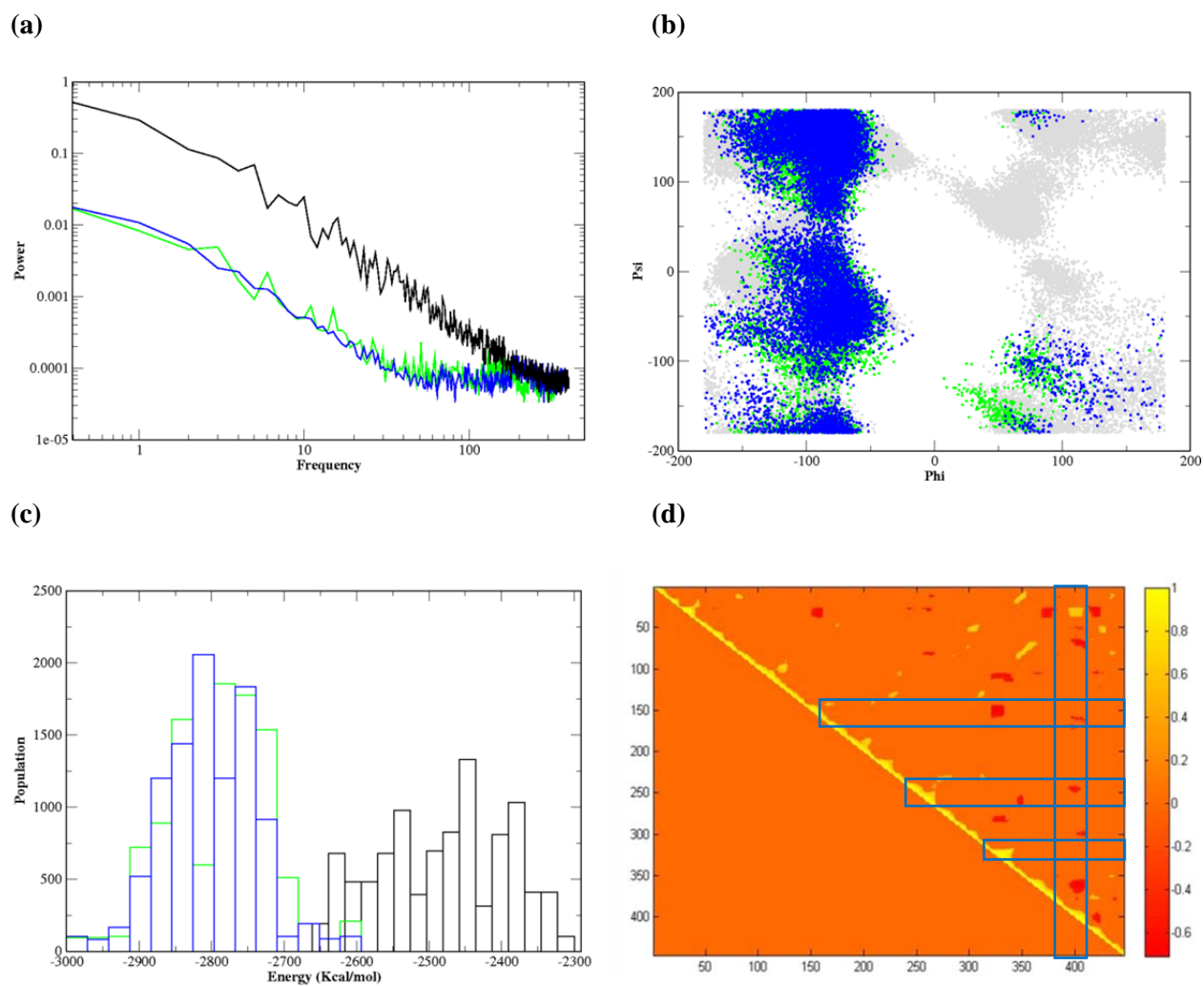
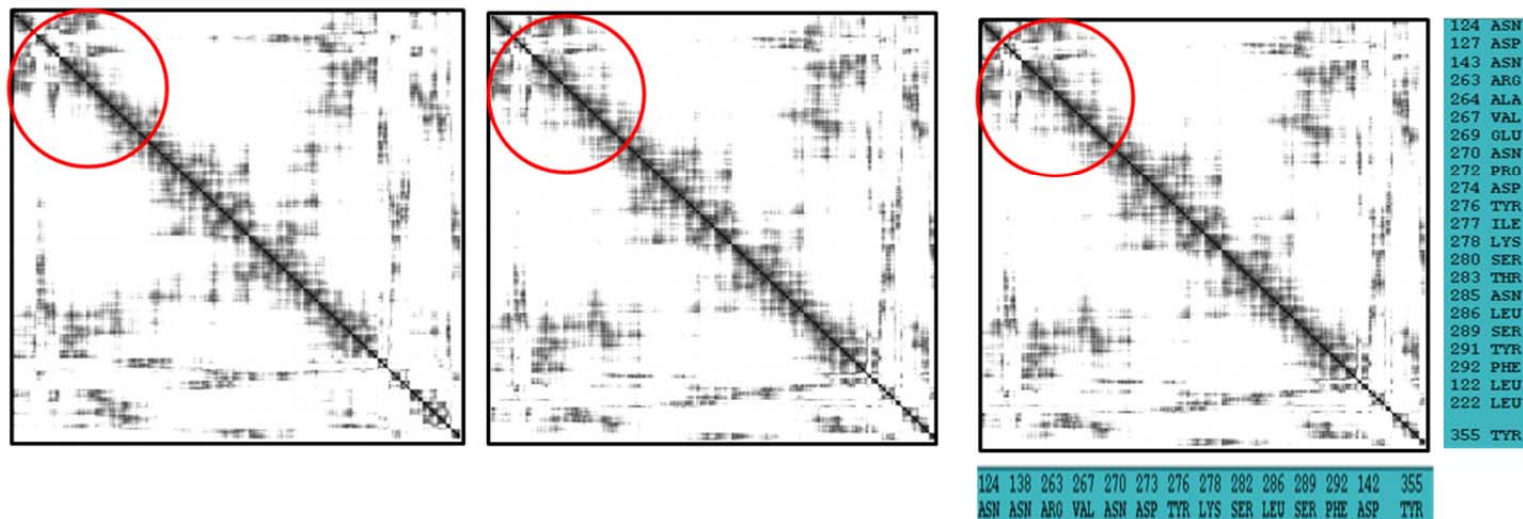


Figure S9. Epitope structure and dynamics in the curved silica-pentamer construct characterized via (a) power spectrum for the fluctuations, (b) the backbone dihedral distribution and (c) energetics of inter-epitope interactions. Using the color-code of Figures 6 and S8, results imply, the power, dihedral distribution and inter-epitope interaction energy of FG shows excellent agreement between silica-based design and the T=1 VLP. Decrease in power and dihedral spread, and increase in interaction energies also imply FG motions are restricted relative to the monomer. (d) As in Figure 4, the epitope-h4 correlations are much lesser than in an L1 monomer or pentamer.

(a)



(b)

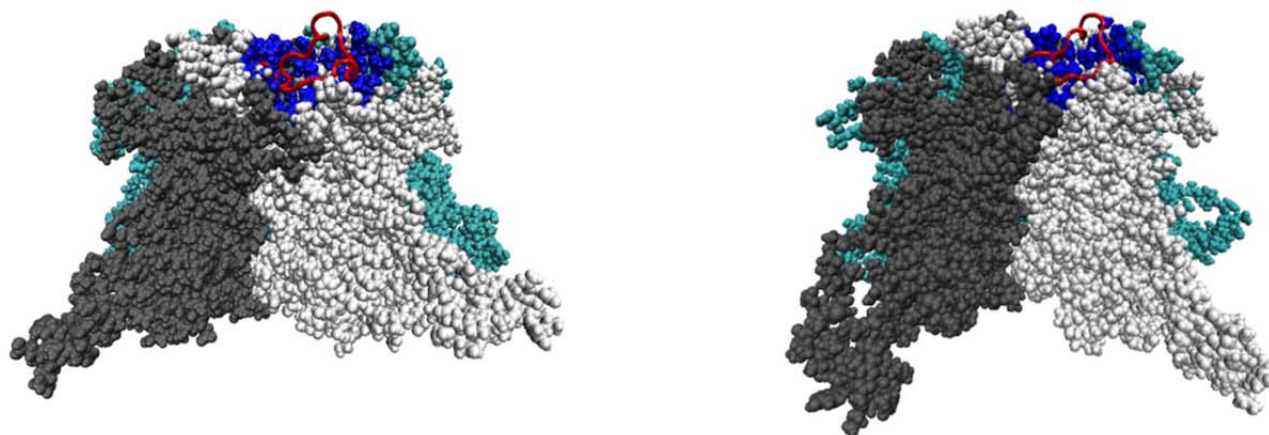


Figure S10. (a) Contact map analysis showing FG is similarly embedded among the surface exposed residues in the complete VLP and design G. (b) Some of the contacts with DE and HI are lost, as FG becomes more solvent accessible when curvature of the silica surface is not maintained, as also presented in Figure S8.

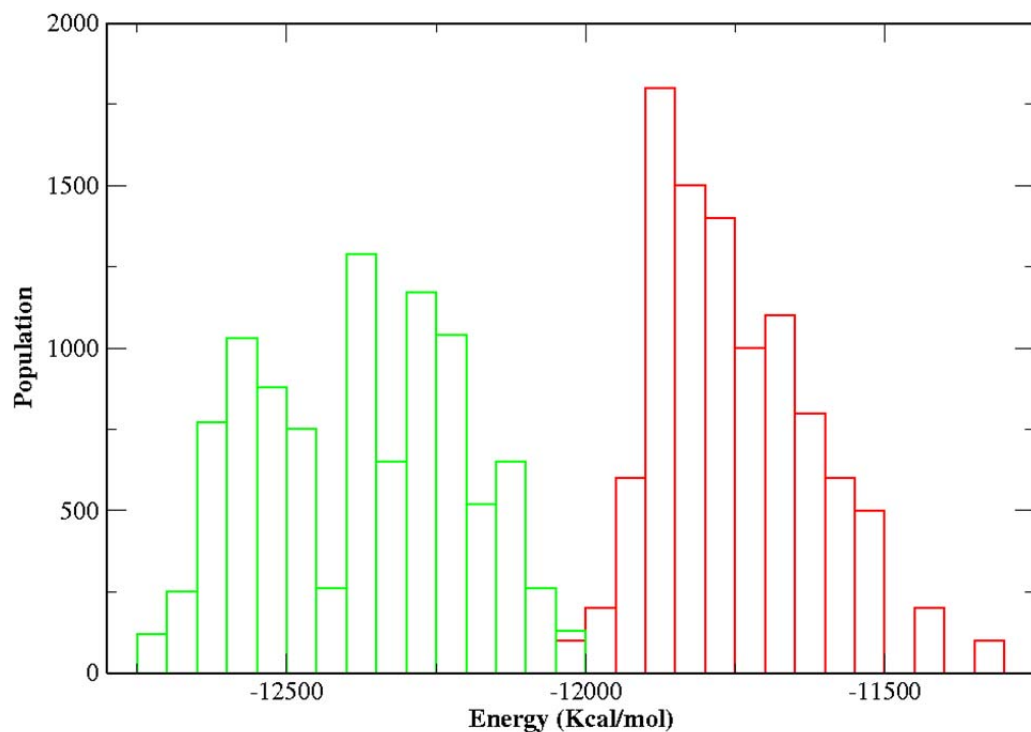


Figure S11. h4 helix-silica interactions (green) as the L1 pentamer is attached to the curved silica are stronger than inter-h4 interactions (red) present in the T=1 HPV VLP. This enthalpic gain in inter-subunit stabilization enables stability of the proposed design.

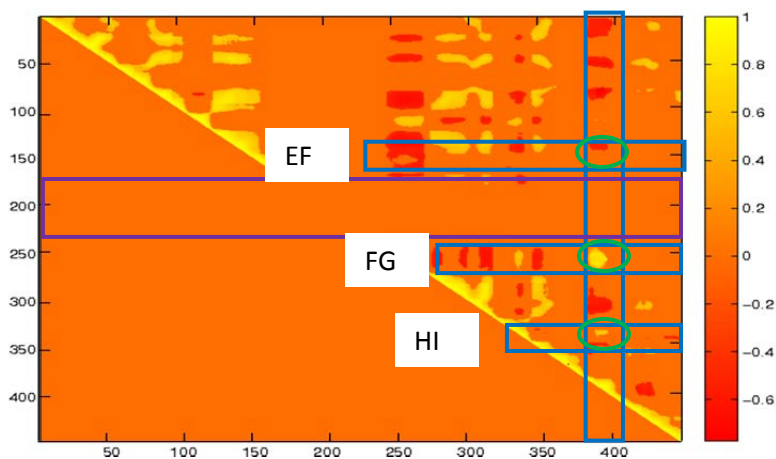


Figure S12. h4-epitope correlations (green circles), Amino acids 169- 239 artificially rigidified (region in purple).

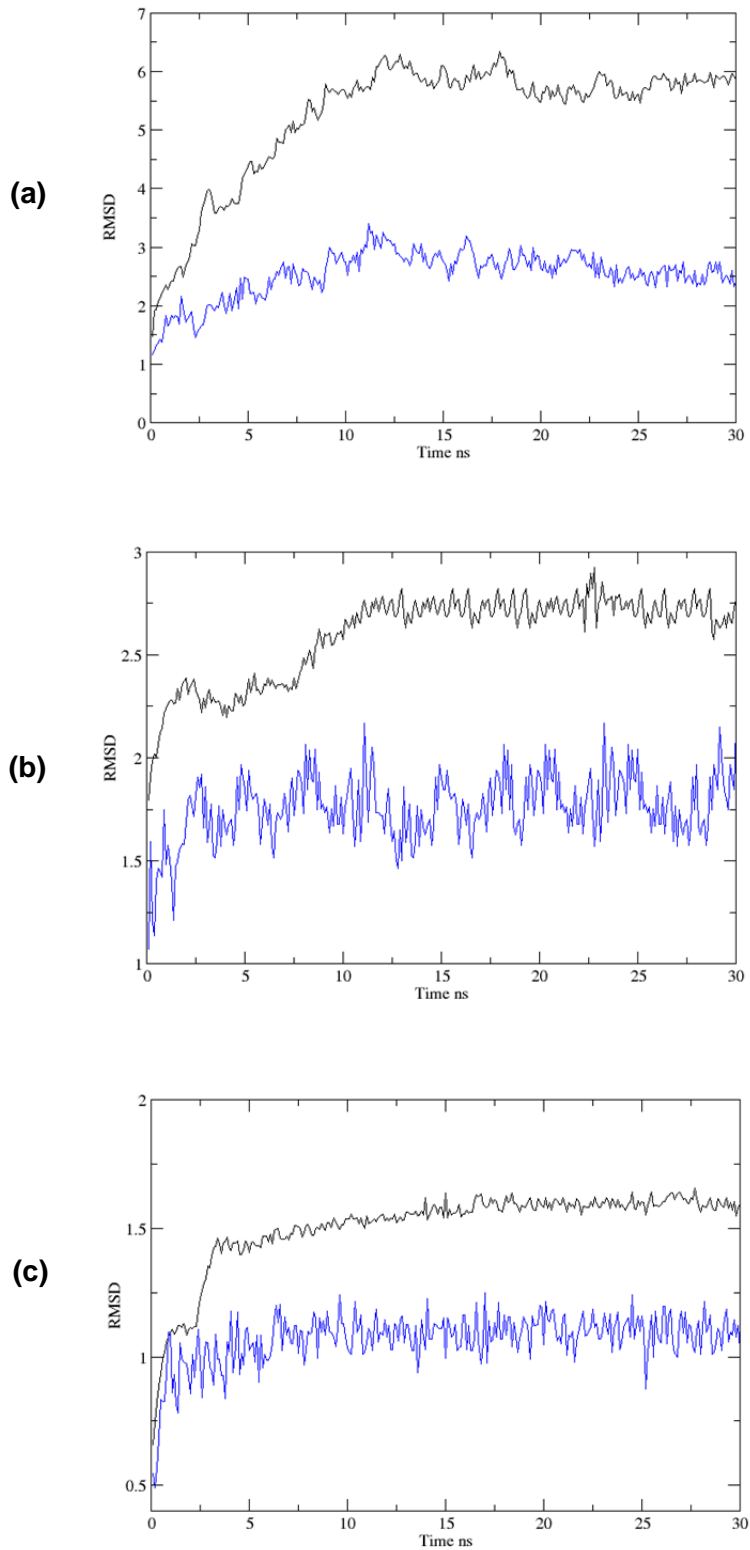


Figure S13. RMSD(Å) plots of (a) L1 monomer(black) FG loop in monomer(blue) (b) Silica-Pentamer(black) FG loop in pentamer(blue) (c) T = 1 VLP(black) FG loop in T=1 VLP(blue).

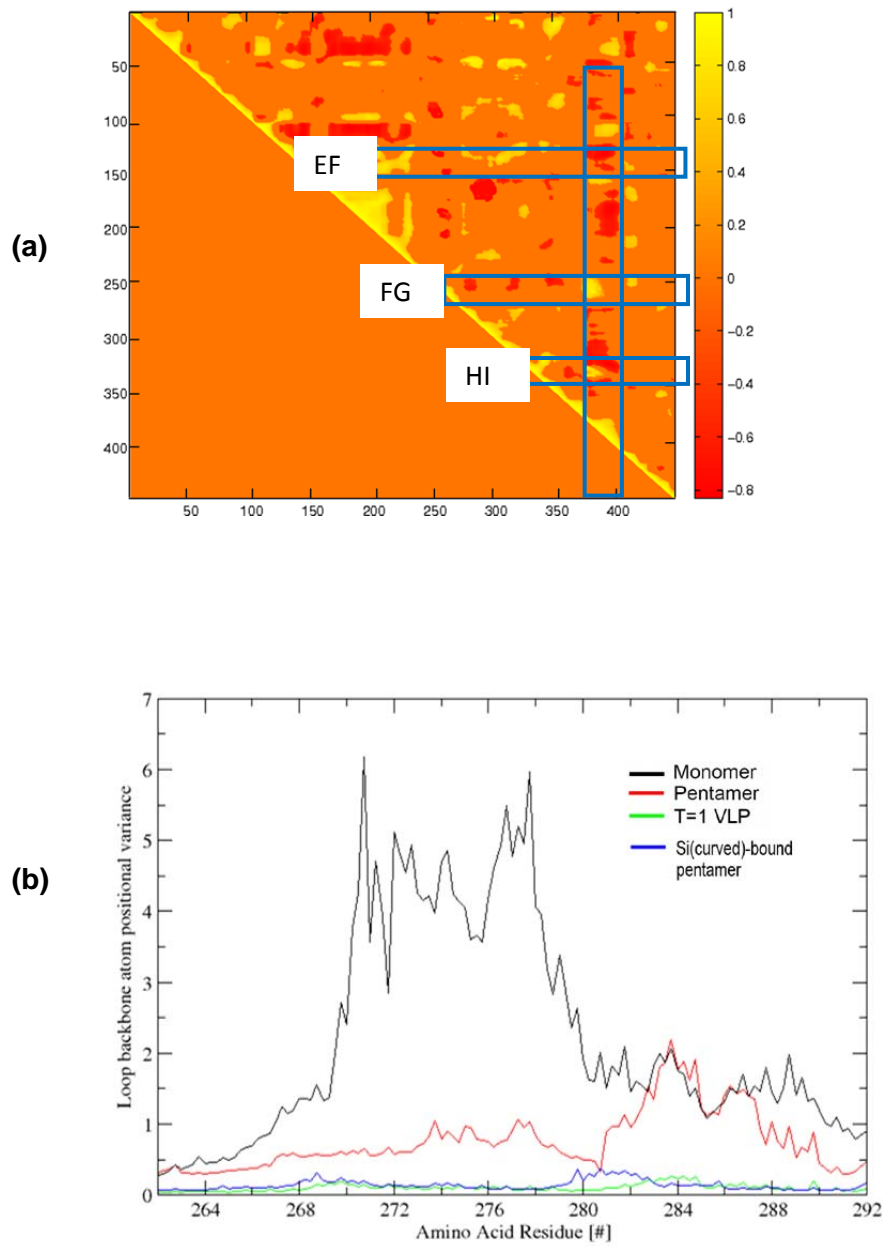


Figure S14. (a) Correlation plot with 5ns data (b) Loop backbone atom positional variance(\AA^2) with 5ns data for FG loop.

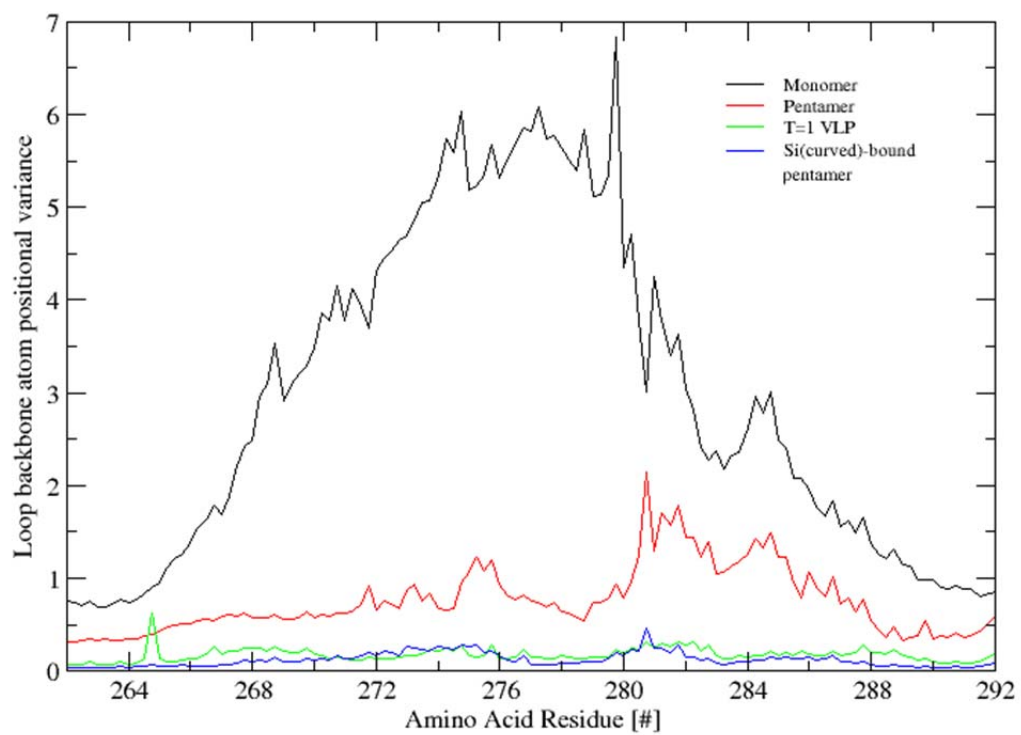


Figure S15. Loop backbone atom positional variance(\AA^2) with 30ns data for FG loop.

Table S2. Force field parameter file for the tether attached to silica and protein.

MASS 201 CR 12.011000	CR NC=O C=O 59.084 119.6000
MASS 202 NC=O 14.006700	CR NC=O HNCO 39.725 120.0660
MASS 203 SI 28.085500	C=O NC=O HNCO 41.380 120.2770
MASS 204 HCMM 1.007940	HCMM SI HCMM 18.567 108.6990
MASS 205 C=O 12.011000	HCMM SI OR 37.422 109.6770
MASS 206 HNCO 1.007940	NC=O C=O CR 70.814 112.7350
MASS 207 O=C 15.999400	NC=O C=O O=C 65.273 127.1520
MASS 208 OR 15.999400	CR C=O O=C 67.504 124.4100
BONDS	C=O CR HCMM 46.778 108.3850
CR CR 306.432 1.5080	CR OR SI 78.658 114.9430
CR HCMM 342.991 1.0930	OR SI OSiE 30.000 121.5000
CR OR 363.214 1.4180	DIHEDRALS
CR NC=O 335.651 1.4360	CR CR CR NC=O 0.150 3 0.00
C=O CR 301.539 1.4920	CR CR CR HCMM 0.320 1 0.00
C=O NC=O 419.491 1.3690	CR CR CR HCMM -0.315 2 180.00
C=O O=C 931.963 1.2220	CR CR CR HCMM 0.132 3 0.00
HCMM SI 162.212 1.4850	CR OR SI HCMM 0.075 3 0.00
HNCO NC=O 479.511 1.0150	CR OR SI OSiE 0.075 3 0.00
OR SI 335.435 1.6600	CR CR OR SI 0.100 3 0.00
ANGLES	CR CR NC=O C=O -0.513 1 0.00
CR CR HCMM 45.770 110.5490	CR CR NC=O C=O 0.347 2 180.00
CR CR OR 71.390 108.1330	CR CR NC=O C=O 0.474 3 0.00
HCMM CR HCMM 37.134 108.8360	CR CR NC=O HNCO 0.276 1 0.00
HCMM CR OR 56.205 108.5770	CR CR NC=O HNCO -0.190 2 180.00
CR CR CR 61.243 109.6080	CR CR NC=O HNCO 0.163 3 0.00
CR CR NC=O 75.564 109.9600	CR CR CR OR -0.344 1 0.00
NC=O CR HCMM 53.255 107.6460	CR CR CR OR 0.878 2 180.00

CR CR CR OR	0.238	3	0.00	HCMM CR CR OR	-0.327	1	0.00
CR NC=O C=O CR	0.324	1	0.00	HCMM CR CR OR	0.536	2	180.00
CR NC=O C=O CR	3.079	2	180.00	HCMM CR CR OR	0.140	3	0.00
CR NC=O C=O CR	0.254	3	0.00	O=C C=O CR HCMM	0.330	1	0.00
CR NC=O C=O O=C	-0.160	1	0.00	O=C C=O CR HCMM	-0.704	2	180.00
CR NC=O C=O O=C	3.147	2	180.00	O=C C=O CR HCMM	0.154	3	0.00
CR NC=O C=O O=C	-0.073	3	0.00	Si OSiE Si OR	0.180	5	0.00
NC=O CR CR HCMM	0.213	3	0.00	IMPROPER			
NC=O C=O CR HCMM	-0.206	1	0.00	CR OR CR HCMM	0.000	0	0.00
NC=O C=O CR HCMM	0.346	2	180.00	CR HCMM CR HCMM	0.000	0	0.00
NC=O C=O CR HCMM	0.043	3	0.00	CR CR CR HCMM	0.000	0	0.00
SI OR CR HCMM	0.100	3	0.00	CR NC=O CR HCMM	0.000	0	0.00
C=O NC=O CR HCMM	-1.050	1	0.00	SI HCMM OR HCMM	0.000	0	0.00
C=O NC=O CR HCMM	0.681	2	180.00	NC=O C=O CR HNCO	-1.439	0	0.00
C=O NC=O CR HCMM	0.011	3	0.00	C=O O=C NC=O CR	9.284	0	0.00
HNCO NC=O CR HCMM	-0.308	1	0.00	CR HCMM C=O HCMM	0.000	0	0.00
HNCO NC=O CR HCMM	0.137	3	0.00	NONBONDED			
HNCO NC=O C=O CR	-0.147	1	0.00	CR	0.000000	-0.055000	2.175000
HNCO NC=O C=O CR	2.902	2	180.00		0.000000	-0.010000	1.900000
HNCO NC=O C=O CR	0.671	3	0.00	NC=O	0.000000	-0.200000	1.850000
HNCO NC=O C=O O=C	0.718	1	0.00	SI	0.000000	-0.310000	2.500000
HNCO NC=O C=O O=C	2.487	2	180.00	HCMM	0.000000	-0.022000	1.320000
HNCO NC=O C=O O=C	-0.227	3	0.00	C=O	0.000000	-0.110000	2.000000
HCMM CR CR HCMM	0.142	1	0.00	HNCO	0.000000	-0.046000	0.224500
HCMM CR CR HCMM	-0.693	2	180.00	O=C	0.000000	-0.120000	1.700000
HCMM CR CR HCMM	0.157	3	0.00		0.000000	-0.120000	1.400000
				OR	0.000000	-0.152100	1.770000

References

- (1) Lopes, P. E. M.; Murashov, V.; Tazi, M.; Demchuk, E.; MacKerell, A. D., *J. Phys. Chem. B* **2006**, *110*, 2782-2792.
- (2) Jaguar, version 7.0, Schrödinger, LLC, New York, NY, 2011.
- (3) Becke, A. D., *J. Chem. Phys.* **1993**, *98*, 5648-5652.
- (4) Lee, C.; Yang, W.; Parr, R. G., *Phys. Rev. B: Condens. Matter Mater. Phys.* **1988**, *37*, 785-789.
- (5) Foloppe, N.; MacKerell, A. D., *J. Comput. Chem.* **2000**, *21*, 86-104.
- (6) Vanommeslaeghe, K.; MacKerell, A. D., Jr., *J. Chem. Inf. Model.* **2012**, *52*, 3144-3154.
- (7) Vanommeslaeghe, K.; Raman, E. P.; MacKerell, A. D., Jr., *J. Chem. Inf. Model.* **2012**, *52*, 3155-3168.
- (8) Besler, B. H.; Merz, K. M.; Kollman, P. A., *J. Comput. Chem.* **1990**, *11*, 431-439.
- (9) Frisch, M. J.; Trucks, G. W.; Schlegel, H. B.; Scuseria, G. E.; Robb, M. A.; Cheeseman, J. R.; Montgomery, J. A.; Vreven, T.; Kudin, K. N.; Burant, J. C.; Millam, J. M.; Iyengar, S. S.; Tomasi, J.; Barone, V.; Mennucci, B.; Cossi, M.; Scalmani, G.; Rega, N.; Petersson, G. A.; Nakatsuji, H.; Hada, M.; Ehara, M.; Toyota, K.; Fukuda, R.; Hasegawa, J.; Ishida, M.; Nakajima, T.; Honda, Y.; Kitao, O.; Nakai, H.; Klene, M.; Li, X.; Knox, J. E.; Hratchian, H. P.; Cross, J. B.; Bakken, V.; Adamo, C.; Jaramillo, J.; Gomperts, R.; Stratmann, R. E.; Yazyev, O.; Austin, A. J.; Cammi, R.; Pomelli, C.; Ochterski, J. W.; Ayala, P. Y.; Morokuma, K.; Voth, G. A.; Salvador, P.; Dannenberg, J. J.; Zakrzewski, V. G.; Dapprich, S.; Daniels, A. D.; Strain, M. C.; Farkas, O.; Malick, D. K.; Rabuck, A. D.; Raghavachari, K.; Foresman, J. B.; Ortiz, J. V.; Cui, Q.; Baboul, A. G.; Clifford, S.; Cioslowski, J.; Stefanov, B. B.; Liu, G.; Liashenko, A.; Piskorz, P.; Komaromi, I.; Martin, R. L.; Fox, D. J.; Keith, T.; Laham, A.; Peng, C. Y.; Nanayakkara, A.; Challacombe, M.; Gill, P. M. W.; Johnson, B.; Chen, W.; Wong, M. W.; Gonzalez, C.; Pople, J. A., Gaussian 03, Revision C.02. In 2003.
- (10) Phillips, J. C.; Braun, R.; Wang, W.; Gumbart, J.; Tajkhorshid, E.; Villa, E.; Chipot, C.; Skeel, R. D.; Kalé, L.; Schulten, K., *J. Comput. Chem.* **2005**, *26*, 1781-1802.
- (11) MacKerell, A. D.; Banavali, N.; Foloppe, N., *Biopolymers* **2000**, *56*, 257-265.
- (12) Jorgensen, W. L.; Chandrasekhar, J.; Madura, J. D.; Impey, R. W.; Klein, M. L., *J. Chem. Phys.* **1983**, *79*, 926-935.
- (13) Feller, S. E.; Zhang, Y. H.; Pastor, R. W.; Brooks, B. R., *J. Chem. Phys.* **1995**, *103*, 4613-4621.
- (14) Vertegel, A. A.; Siegel, R. W.; Dordick, J. S., *Langmuir* **2004**, *20*, 6800-6807.
- (15) Knopp, D.; Tang, D.; Niessner, R., *Anal. Chim. Acta* **2009**, *647*, 14-30.
- (16) Sperling, R. A.; Parak, W. J., *Philos. Trans. R. Soc., A* **2010**, *368*, 1333-1383.
- (17) Aubin-Tam, M. E.; Hamad-Schifferli, K., *Biomed. Mater.* **2008**, *3*, 034001.
- (18) Aubin-Tam, M.-E. H., W.; Hamad-Schifferli, K., *Proc. Nat. Acad. Sci.* **2009**, *106*, 4095-4100.
- (19) Jin, Y.; Li, A.; Hazelton, S. G.; Liang, S.; John, C. L.; Selid, P. D.; Pierce, D. T.; Zhao, J. X., *Coord. Chem. Rev.* **2009**, *253*, 2998-3014.
- (20) Cruz-Chu, E. R.; Aksimentiev, A.; Schulten, K., *J. Phys. Chem. B* **2006**, *110*, 21497-21508.
- (21) Katz, E.; Willner, I., *Angew. Chem. Int. Ed.* **2004**, *43*, 6042-6108.
- (22) Guo, H. C.; Feng, X. M.; Sun, S. Q.; Wei, Y. Q.; Sun, D. H.; Liu, X. T.; Liu, Z. X.; Luo, J. X.; Yin, H., *Virology J.* **2012**, *9*.
- (23) Tsai, C.-J.; del Sol, A.; Nussinov, R., *J. Mol. Biol.* **2008**, *378*, 1-11.
- (24) Daily, M. D.; Gray, J. J., *Proteins: Struct., Funct., Bioinf.* **2007**, *67*, 385-399.
- (25) Hawkins, R. J.; McLeish, T. C. B., *J. R. Soc., Interface* **2006**, *3*, 125-138.